Available online at www.sciencedirect.com

ScienceDirect

IFAC Papers Online CONFERENCE PAPER ARCHIVE

IFAC PapersOnLine 52-14 (2019) 7–12

Feed Size Distribution Feedforward Control for a Grinding Mill Circuit

M. G. Maritz * **J. D. le Roux** * **I. K. Craig** *

* *Department of Electrical, Electronic and Computer Engineering, University of Pretoria, Pretoria, South Africa. (e-mail: ian.craig@up.ac.za)*

Abstract: This paper proposes a method to measure and reject disturbances caused by changes in the ore distribution of the feed to a grinding mill circuit. A computer vision system is presented to measure the fraction of rocks in the feed, using only basic equipment and algorithms. A feedforward controller is designed to reject the measured feed size disturbance within the mill before causing further disturbances downstream. The feedforward controller is implemented in simulation to control a nonlinear mill model, and is compared to conventional feedback control. The allowable plant-model mismatch and practicality of feedforward control for industrial applications are investigated. It was found that feedforward control has a noticeable advantage over feedback control if well tuned. The most significant disturbance is the efficiency of the mill to break ore into fine material. Since this is not currently measured in real-time, it limits the performance of a feedforward controller in practice.

Keywords: Grinding mill circuit, run-of-mine ore, feedforward control, image processing

1. INTRODUCTION

A run-of-mine (ROM) milling circuit plays a vital role in extracting valuable minerals from mined ore. The mill is responsible for grinding and breaking mined ore down to a size small enough that minerals can be extracted by downstream processes. The milling process is difficult to control due to large input disturbances. The main input disturbances are variations in the size distribution and hardness of the ROM ore fed to the mill (Coetzee et al., 2010).

Commercial camera systems are available to measure the size distribution of the feed ore to a mill. This paper investigates how well basic equipment and algorithms can perform such a task in real time. Based on this measurement, a feedforward controller is designed to reject disturbances caused by size distribution changes. The feedforward controller is implemented in simulation to control a grinding mill circuit represented by a nonlinear model (le Roux et al., 2013). The performance of the feedforward controller is compared to a conventional feedback controller. The sensitivity of the feedforward controller to parameter variation is investigated to determine if the controller is fit for industrial applications.

2. CIRCUIT AND MODEL DESCRIPTION

The grinding mill circuit and model used to test the performance of feedforward control is described next. The grinding mill shown in Fig. 1 consists of three elements: mill, sump and hydrocyclone. The mill is supplied with mined ore (MFO), water (MIW), steel balls (MFB) and underflow from the hydrocyclone. The variable $LOAD$ represents the volume of total ore, water, and balls within the mill. The water and ground ore forms a slurry inside

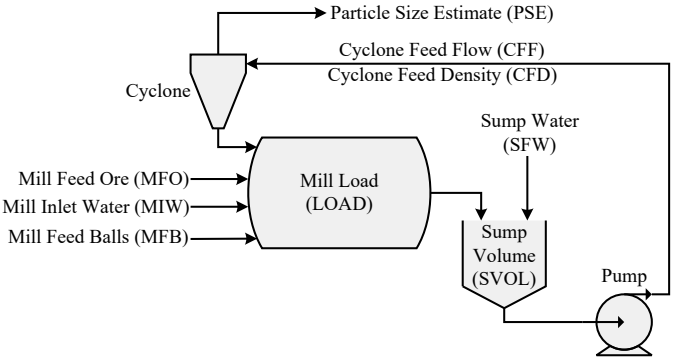

Fig. 1. A single-stage grinding mill circuit.

the mill, which is discharged through an end discharge screen which limits the particle size of the slurry leaving the mill. The slurry enters the sump, where it is diluted with water (SFW) before it is pumped to the cyclone for classification. The slurry volume in the sump and flowrate of slurry to the cyclone is represented by $SVOL$ and CFF respectively. The hydrocyclone separates the in-specification ore from the out-of-specification ore and passes it to the overflow and underflow of the cyclone respectively. The underflow of the hydrocyclone is returned to the mill inlet for further grinding whereas the overflow (PSE) contains the final product which is passed to downstream processes (Napier-Munn et al., 1999). The manipulated and controlled variables of the circuit in Fig. 1 are described in Table 1.

The circuit in Fig. 1 is described by the nonlinear model known as the Hulbert model (le Roux et al., 2013). The model divides the circuit into four modules: a feeder, a semi-autogenous (SAG) mill, a sump and a hydrocyclone.

10.1016/j.ifacol.2019.09.155

Table 1. Description of circuit variables

Manipulated Variables	
MIW	Flow-rate of water to the mill [m^3/h]
MFO	Feed-rate of ore to the mill [t/h]
MFB	Feed-rate of steel balls to the mill [t/h]
SFW	Flow-rate of water to the sump [m^3/h]
CFF	Flow-rate of slurry into classifier [m^3/h]
Controlled Variables	
$LOAD$	Volume of charge within the mill [m^3]
$SVOL$	Volume of slurry in the sump [m^3]
PSE	Product particle size estimate [-]

The aim of the model is to produce reasonably accurate responses while using as few parameters as possible.

The contents of the mill is represented by five states: rocks, solids, fines, balls and water. Rocks are ore too large to leave the mill through the end-discharge screen, whereas solids can leave through the screen. The solids are the sum of fine and coarse ore, where fines is ore smaller than the product specification size, and coarse ore is larger than the specification size. Steel balls are added to aid in breaking ore inside the mill. The balls are too large to leave the mill through the end-discharge screen.

In the equations that follow, X denotes the states of the model as volumes in m^3 and V denotes a flow-rate in m^3/h. The first subscript indicates the module of interest, the second is the state considered, and the third indicates an inflow, overflow or underflow (in the case of flow-rate). A more detailed description of the subscripts for X and V is provided in Table 2.

Table 2. Description of subscripts

Subscript	Description
$X_{\square\_}$	f-feeder; m-mill; s-sump; c-cyclone
$X_{\_\square}$	w-water; s-solids; c-coarse; f-fines; r-rocks; b-balls
$V_{\_\_\square}$	i-inflow; o-outflow; u-underflow

The parameters used in the model are described in Table 3. The values used in this article were taken from le Roux et al. (2013). The continuous-time state-space description of the grinding mill circuit is shown below:

$$\dot{X}_{mr} = \frac{MFO}{D_S}\alpha_r - \frac{P_{mill}\varphi}{D_S\phi_r}\left(\frac{X_{mr}}{X_{mr}+X_{ms}}\right) \tag{1a}$$

$$\dot{X}_{ms} = \frac{MFO}{D_S}(1-\alpha_r) - \frac{V_V\varphi X_{mw}X_{ms}}{X_{ms}+X_{mw}} + V_{csu} + \frac{P_{mill}\varphi}{D_S\phi_r}\left(\frac{X_{mr}}{X_{mr}+X_{ms}}\right) \tag{1b}$$

$$\dot{X}_{mf} = \frac{MFO}{D_S}\alpha_f - \frac{V_V\varphi X_{mw}X_{mf}}{X_{ms}+X_{mw}} + V_{cfu} + \frac{P_{mill}}{D_S\phi_f}/\left[1+\alpha_{\phi_f}\left(\frac{X_{mw}+X_{mr}+X_{ms}+X_{mb}}{v_{mill}} - v_{P_{max}}\right)\right] \tag{1c}$$

$$\dot{X}_{mb} = \frac{MFB}{D_B} - \frac{P_{mill}\varphi}{\phi_b}\left(\frac{X_{mb}}{D_S\left(X_{mr}+X_{ms}\right)+D_BX_{mb}}\right) \tag{1d}$$

$$\dot{X}_{mw} = MIW - \frac{V_V\varphi X_{mw}X_{mw}}{X_{ms}+X_{mw}} + V_{cwu} \tag{1e}$$

$$\dot{X}_{ss} = \frac{V_V\varphi X_{mw}X_{ms}}{X_{ms}+X_{mw}} - \frac{CFFX_{ss}}{X_{sw}+X_{ss}} \tag{1f}$$

$$\dot{X}_{sf} = \frac{V_V\varphi X_{mw}X_{mf}}{X_{ms}+X_{mw}} - \frac{CFFX_{sf}}{X_{sw}+X_{ss}} \tag{1g}$$

$$\dot{X}_{sw} = \frac{V_V\varphi X_{mw}X_{mw}}{X_{ms}+X_{mw}} - \frac{CFFX_{sw}}{X_{sw}+X_{ss}} + SFW \tag{1h}$$

where the volume of rocks, solids, fines, balls, and water in the mill are represented by X_{mr}, X_{ms}, X_{mf}, X_{mb} and X_{mw} respectively. The volume of solids, fines, and water within the sump are represented by X_{ss}, X_{sf} and X_{sw} respectively.

Table 3. Feeder, mill and cyclone parameters

Parameter	Value	Description
α_f	0.055	Fraction fines in the feed ore
α_r	0.465	Fraction rock in the feed ore
α_P	1.0	Fractional power reduction per fractional reduction from maximum mill speed
α_{ϕ_f}	0.01	Fractional change in kW/fines produced per change in fractional filling of mill
α_{speed}	0.71	Fraction of critical mill speed
δ_{P_s}	0.5	Power-change parameter for fraction solids in the mill
δ_{P_v}	0.5	Power-change parameter for volume of mill filled
D_B	7.85	Density of steel balls [t/m^3]
D_S	3.2	Density of feed ore [t/m^3]
ε_{sv}	0.6	Maximum fraction solids by volume of slurry at 0 slurry flow
ϕ_b	90.0	Steel consumption factor [kWh/t]
ϕ_f	29.6	Fines production factor [kWh/t]
ϕ_r	6.03	Rock consumption factor [kWh/t]
$\varphi_{P_{max}}$	0.57	Rheology factor for maximum mill power
P_{max}	1662	Maximum mill motor power draw [kW]
v_{mill}	59.12	Mill volume [m^3]
$v_{P_{max}}$	0.34	Fraction of mill volume filled for maximum power draw
V_V	84.0	Volumetric flow per "flowing volume" driving force [h^{-1}]
α_{su}	0.87	Parameter for fraction solids in underflow
C_1	0.6	Constant
C_2	0.7	Constant
C_3	4.0	Constant
C_4	4.0	Constant
ε_c	129	Parameter related to coarse split [m^3/h]

The parameters α_r and α_f represent the volumetric fraction of rocks and fines in the feed ore respectively. These two parameters serve as a very rough indication of the feed-size distribution.

The parameter ϕ_r is the rock consumption factor and indicates the energy required to break a tonne of rocks down to solids. The parameter ϕ_f is the fines production factor and indicates the energy required to produce a tonne of fines. These two parameters indicate the efficiency of the mill to break ore. They are dependent on both the hardness of the ore (Morrell, 2004; Hinde and Kalala, 2009), as well as the feed size distribution (Morrell et al., 1996; Morrell and Valery, 2001; Fang et al., 2018).

The intermediate equations required in (1) are

$$\varphi = \left(1-\left(\frac{1}{\varepsilon_{sv}}-1\right)\frac{X_{ms}}{X_{mw}}\right)^{0.5} \tag{2a}$$

$$P_{mill} = P_{max}\{1-\delta_{Pv}Z_x^2-\delta_{Ps}Z_r^2\}\cdot(\alpha_{speed})^{\alpha_P} \tag{2b}$$

$$Z_x = \frac{X_{mw}+X_{mr}+X_{ms}+X_{mb}}{v_{mill}v_{P_{max}}} - 1 \tag{2c}$$

$$Z_r = \frac{\varphi}{\varphi_{P_{max}}} - 1 \tag{2d}$$

where P_{mill} is the power draw of the mill, Z_x models the effect of the charge fill on the mill power draw, Z_r models the effect of rheology of the charge on the power draw, and φ is an empirically defined rheology factor of the charge within the mill. The output equations are

$$LOAD = X_{mr} + X_{ms} + X_{mb} + X_{mw} \tag{3a}$$
$$SVOL = X_{ss} + X_{sw} \tag{3b}$$
$$PSE = \frac{V_{cfo}}{V_{cso}} \tag{3c}$$

where V_{cso} and V_{cfo} are the volumetric flow rate of solids and fines at the cyclone overflow respectively. The intermediate equations required in (1) and (3) related to the cyclone are

$$F_u = 0.6 - \left(0.6 - \frac{X_{ss}}{X_{sw}+X_{ss}}\right)\exp\left(\frac{-V_{ccu}}{\alpha_{su}\varepsilon_c}\right) \tag{4a}$$
$$V_{csu} = V_{ccu} + \frac{X_{sf}\left(V_{ccu} - F_u V_{ccu}\right)}{F_u X_{sw} + F_u X_{sf} - X_{sf}} \tag{4b}$$
$$V_{ccu} = \frac{CFF\left(X_{ss} - X_{sf}\right)}{X_{sw}+X_{ss}}\left(1 - C_1 e^{\left(\frac{-CFF}{\varepsilon_c}\right)}\right) \times \tag{4c}$$
$$\left(1 - \left(\frac{X_{ss}}{C_2\left(X_{sw}+X_{ss}\right)}\right)^{C_3}\right)\left(1 - \left(\frac{X_{sf}}{X_{ss}}\right)^{C_4}\right) \tag{4d}$$
$$V_{cfu} = \frac{X_{sf}\left(V_{ccu} - F_u V_{ccu}\right)}{F_u X_{sw} + F_u X_{sf} - X_{sf}} \tag{4e}$$
$$V_{cwu} = \frac{X_{sw}\left(V_{ccu} - F_u V_{ccu}\right)}{F_u X_{sw} + F_u X_{sf} - X_{sf}} \tag{4f}$$
$$V_{cso} = V_{sso} - V_{csu} \tag{4g}$$
$$V_{cfo} = V_{sfo} - V_{cfu} \tag{4h}$$
$$V_{sso} = CFF\frac{X_{ss}}{X_{ss} - X_{sw}} \tag{4i}$$
$$V_{sfo} = CFF\frac{X_{sf}}{X_{ss} - X_{sw}} \tag{4j}$$

where the fraction of solids in the cyclone underflow is represented by F_u. The flow-rate of solids, fines and water at the underflow of the cyclone is represented by V_{csu}, V_{cfu} and V_{cwu} respectively, and the flow-rate of solids and fines at the sump outflow is V_{sso} and V_{sfo} respectively.

3. MEASUREMENT OF SIZE DISTRIBUTION

The fraction of rocks in the ore fed to the mill, α_r, is measured by means of a camera taking pictures of the ore before it enters the mill. The images are processed in Python, using the open source computer vision package, OpenCV.

The process to calculate α_r from a camera image is explained with the use of Fig. 2. (This study only considers a static, single layer of ore in a laboratory setting. Future work will investigate the calculation of α_r from multiple layers of moving ore as found in an industrial circuit.)

- Fig. 2a: In the initial image the ore is distributed such that a black background is visible between them.
- Fig. 2b: The image is converted to grayscale and filtered to remove noise, after which a threshold is applied based on the brightness of each pixel. The resulting binary image has either white (foreground) pixels, or black (background) pixels. Morphological opening (Dougherty and Lotufo, 2003) is applied to the binary image, which first shrinks the foreground, and then expands it back to its original size. This has the effect of the background swallowing small foreground spots.
- Fig. 2c: With a conditioned binary image, the distance transform (Dougherty and Lotufo, 2003) is applied, which replaces each foreground pixel with a value representing its distance from the nearest background pixel. This creates an image similar to a contour map, from which the local maxima, or peaks, are found. The identification of peaks, known as markers, allows for the identification of the centre of each rock and thus separates them if they share a common boundary. A threshold is applied to the distance transform to set a minimum size for the ore that can be detected. This prevents false detections and erroneous segmentation of touching ore.
- Fig. 2d: The background from the binary image is combined with the markers from the distance transform. The space between the background and the markers is set as a new black background which is used to identify the shape of each individual rock.
- Fig. 2e: The watershed algorithm (Dougherty and Lotufo, 2003) is then applied, which can be visualised as water flowing from each marker. The water floods the black region of Fig. 2d until the water from each marker touch the water from another marker, filling up the black space. The touching boundary is assumed to also be the boundary between ore, allowing identification of the shape and size of each rock. Each colour in the image represents an individual rock.
- Fig. 2f: Lastly, the outside contour and size of each coloured segment in Fig. 2e is calculated as shown by the red contour lines.

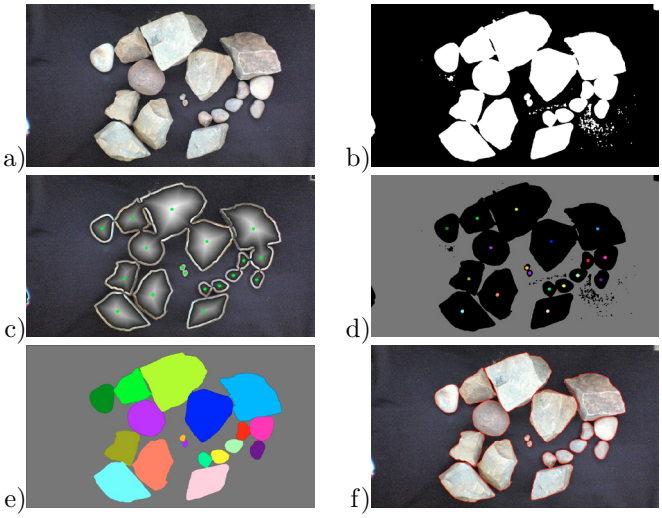

Fig. 2. Image processing steps for ore feed segmentation.

To calculate the fraction of ore that does not fit through a grid with a specific aperture size, the shape of each rock is assumed to be a circle. The circle diameter, d, with equivalent, software determined area, A, is calculated as

$$d = \sqrt{4A/\pi} \tag{5}$$

The ratio, α_r, is calculated as

$$\alpha_r = N^+/N \tag{6}$$

where N^+ is the is the number of rocks in frame with a diameter larger than the grid aperture size and N is the total number of rocks in frame. For a discharge screen with 22.4 mm aperture size, the fraction of rocks in Fig. 2 was calculated as $\alpha_r = 0.61$.

4. CONTROLLER DESIGN

Milling circuits commonly use single-loop Proportional Integral (PI) feedback controllers for control (Wei and Craig, 2009), but these controllers can be slow to respond to disturbances. The challenge for any grinding mill controller is to reject disturbances caused by changes in feed-size distribution and feed ore hardness. To improve the ability of the controllers to reject disturbances in the ore feed size distribution, a feedforward controller is designed.

The system block diagram is shown in Fig. 3. It shows a feedforward (FF), G_{C-FF}, and feedback (FB), G_{C-FB}, controller. The FF controller design is described in Seborg et al. (2011). The disturbance transfer function, G_D, is part of the the nonlinear Hulbert model, but is isolated for design purposes. The design of each controller is described in the sections that follow. All the time constants and time delays are in hours.

4.1 Linear Plant Model

To design and tune the controllers, the nonlinear mill model is linearised at an optimal mill operating point of a real mill circuit. The operating point, taken from le Roux et al. (2013), is shown in Table 4.

The input-output pairing is chosen as: $MFO - LOAD$, $SFW - SVOL$, and $CFF - PSE$ (Coetzee, 2009). Step-tests are applied to the nonlinear model to derive the linear models for these pairs. The linear models are

$$\begin{aligned}\begin{bmatrix} LOAD(s) \\ SVOL(s) \\ PSE(s) \end{bmatrix} &= G_{Pl}(s) \begin{bmatrix} MFO(s) \\ SFW(s) \\ CFF(s) \end{bmatrix} \\ &= \begin{bmatrix} \frac{0.235}{0.7s+1} & 0 & 0 \\ 0 & \frac{0.49}{s} & 0 \\ 0 & 0 & \frac{-0.002}{0.3s+1}e^{-0.1s} \end{bmatrix} \begin{bmatrix} MFO(s) \\ SFW(s) \\ CFF(s) \end{bmatrix}\end{aligned} \tag{7}$$

4.2 Feedback Controller

The linearised model in (7) is used to tune the single-loop PI controllers. The PI controller is tuned to be reasonably fast, but still result in practical values for the inputs. The designed PI feedback controller transfer functions are

$$G_{C-FB}(s) = \begin{bmatrix} (15 + \frac{20}{s}) & 0 & 0 \\ 0 & (20 + \frac{80}{s}) & 0 \\ 0 & 0 & (500 + \frac{5000}{s}) \end{bmatrix} \tag{8}$$

4.3 Feedforward Controller

Parameters α_r and α_f describe the mill feed size distribution. The efficiency of the mill to break ore is a function of both the feed size distribution and the relative hardness of the ore. When the feed size of a SAG mill becomes coarser, i.e. α_r increases, the energy required to break the ore increases, i.e. ϕ_r and ϕ_f increases (Morrell et al., 1996; Morrell and Valery, 2001; Fang et al., 2018). If the relative hardness of the ore increases, both ϕ_r and ϕ_f increases. The feedforward controller is thus designed to include four disturbance variables, α_r, α_f, ϕ_r, and ϕ_f.

Ore feed disturbances will influence the mill charge first, after which the disturbance propagates through the circuit. The FF controller is designed to reject the disturbance in the mill before it can propagate any further. To

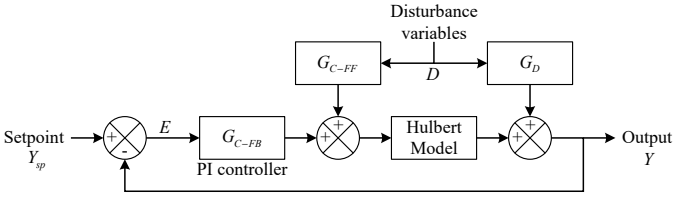

Fig. 3. System block diagram.

Table 4. Milling circuit operating point

Parameter	Value	Units	Parameter	Value	Units
X_{mr}	1.82	m^3	X_{mb}	8.51	m^3
X_{ms}	4.90	m^3	X_{ss}	1.88	m^3
X_{mf}	1.09	m^3	X_{sf}	0.42	m^3
X_{mw}	4.85	m^3	X_{sw}	4.11	m^3
MFO	65.2	t/h	SFW	140.5	m^3/h
MIW	4.64	m^3/h	CFF	374	m^3/h
MFB	5.69	t/h			

design the FF controller, a transfer function is required to quantify the effect of each disturbance variable on the mill output. With the nonlinear model in steady state and all controllers removed from the loop, a step is applied to each disturbance variable individually. The identified transfer functions describing the effect of each disturbance variable on the mill $LOAD$ are

$$\begin{aligned}LOAD(s) &= G_{Dl}(s) \begin{bmatrix} \alpha_r(s) \\ \alpha_f(s) \\ \phi_r(s) \\ \phi_f(s) \end{bmatrix} \\ &= \begin{bmatrix} \frac{3.5}{0.727s+1}e^{-0.278s} \\ \frac{-20}{0.734s+1} \\ \frac{0.25}{0.696s+1}e^{-0.278s} \\ \frac{0.28}{0.725s+1}e^{-0.056s} \end{bmatrix}^T \begin{bmatrix} \alpha_r(s) \\ \alpha_f(s) \\ \phi_r(s) \\ \phi_f(s) \end{bmatrix}\end{aligned} \tag{9}$$

The FF controller transfer functions are

$$\begin{aligned}MFO(s) &= G_{C-FF}(s) \begin{bmatrix} \alpha_r(s) \\ \alpha_f(s) \\ \phi_r(s) \\ \phi_f(s) \end{bmatrix} \\ &= -\begin{bmatrix} \frac{G_{Dl11}}{G_{Pl11}} & \frac{G_{Dl12}}{G_{Pl11}} & \frac{G_{Dl13}}{G_{Pl11}} & \frac{G_{Dl14}}{G_{Pl11}} \end{bmatrix} \begin{bmatrix} \alpha_r(s) \\ \alpha_f(s) \\ \phi_r(s) \\ \phi_f(s) \end{bmatrix} \\ &= \begin{bmatrix} \frac{-14.35s-20.5}{s+1.376}e^{-0.278s} \\ \frac{81.17s+116}{s+1.362} \\ \frac{-1.07s-1.528}{s+1.436}e^{-0.278s} \\ \frac{-1.15s-1.643}{s+1.379}e^{-0.056s} \end{bmatrix}^T \begin{bmatrix} \alpha_r(s) \\ \alpha_f(s) \\ \phi_r(s) \\ \phi_f(s) \end{bmatrix}\end{aligned} \tag{10}$$

The FF controller does not adjust SFW and CFF, but only MFO to reject $LOAD$ disturbances.

5. SIMULATION

5.1 Simulation Environment

The model and controllers were simulated using MATLAB. To evaluate the effect of the FF controller, two control strategies are applied to the nonlinear model described in Section 2: the FB controller only, and the feedback with

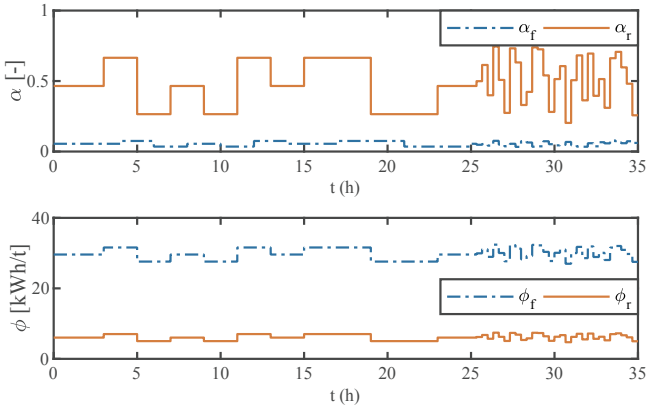

Fig. 4. Applied disturbance variables.

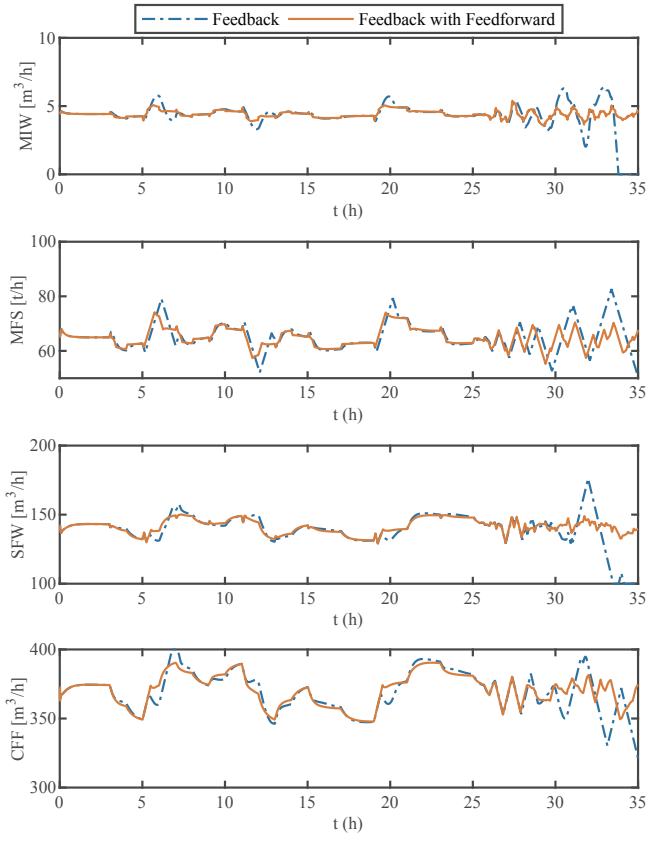

Fig. 5. Mill input variables with feedback and feedback with feedforward (FBFF) controllers implemented.

feedforward (FBFF) controller. The system was allowed to reach steady state, after which steps were applied to the disturbance variables α_r and α_f as shown in Fig. 4. The change in energy required to consume the rocks were included by changing ϕ_r and ϕ_f in proportion to α_r. The disturbances, ϕ_r and ϕ_f cannot be measured in real time meaning that the associated FF controller cannot be implemented. This was remedied by assuming the change, Δ, in ϕ_r and ϕ_f as a ratio of the change in α_r. The ratio for ϕ_r and ϕ_f is represented by x and y respectively. The values for x and y in the simulations are 5 and 10 respectively, but will need to be experimentally determined for real mill circuits. The step sizes applied to the disturbance variables, $D(s)$, are

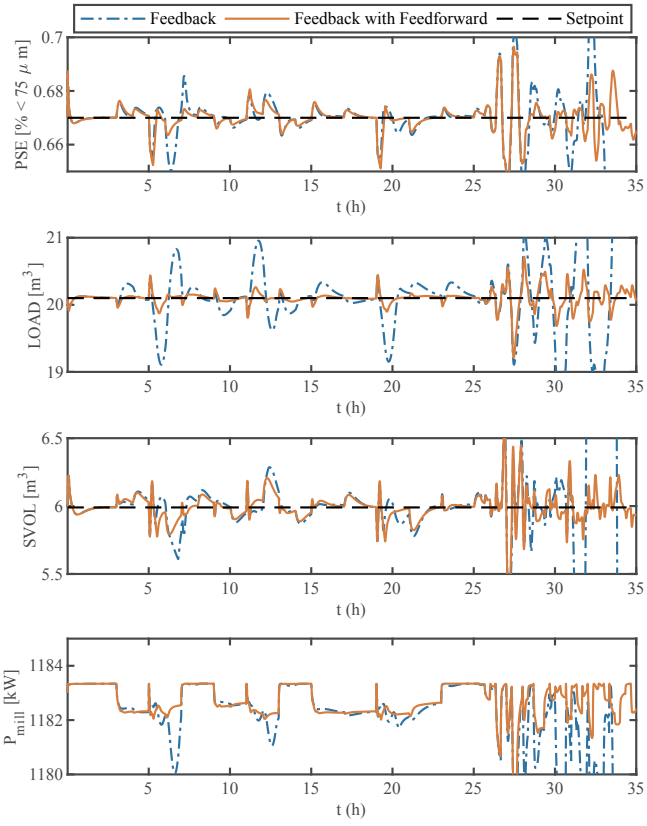

Fig. 6. Mill output variables with feedback and feedback with feedforward (FBFF) controllers implemented.

Table 5. Input constraints

Var	Min	Max	RoC	Description
MIW	0	10	50	Flow-rate of water to the mill [m^3/h]
MFO	50	100	20	Feed-rate of ore to the mill [t/h]
SFW	100	200	50	Flow-rate of water to the sump [m^3/h]
CFF	300	400	50	Cyclone feed flow rate [m^3/h]

$$D(s) = \begin{bmatrix} \alpha_r(s) \pm \Delta\alpha_r(s) \\ \alpha_f(s) \pm \Delta\alpha_f(s) \\ \phi_r(s) \pm x\Delta\alpha_r(s) \\ \phi_f(s) \pm y\Delta\alpha_r(s) \end{bmatrix} = \begin{bmatrix} \alpha_r(s) \pm 0.2 \\ \alpha_f(s) \pm 0.02 \\ \phi_r(s) \pm 5 \times 0.2 \\ \phi_f(s) \pm 10 \times 0.2 \end{bmatrix} \quad (11)$$

The simulation spans a period of 35 h, with a controller sampling time of 10 s. For the first 25 h, constant disturbance step sizes are applied, after which random step sizes are applied every 20 min. The constraints shown in Table 5 were applied to limit the input range and the Rate-of-Change (RoC) per hour to practical values.

5.2 Simulation Results

The manipulated variables are shown in Fig. 5, where the y-axis range is the input range constraint. The applied input RoC constraint was reached several times. The output is shown in Fig. 6. At the 30 h mark, the FBFF controller is able to keep the mill stable under conditions where FB control becomes unstable. Throughout the simulations, it was found that FBFF control could maintain stability for a wider range of disturbance conditions than FB control only.

The simulation data is analysed from $t = 2$ h (after the system settled) to $t = 25$ h (before the unstable region),

Table 6. Simulation analysis for $t = 2 - 25\ h$.

Variable	Feedback	Feedback with Feedforward
Standard deviation		
MIW	0.391	0.250
MFS	4.34	3.50
SFW	6.97	5.87
CFF	14.3	13.2
Root mean squared error (RMSE)		
PSE	4.58 e-3	3.50 e-3
$LOAD$	29.5 e-2	6.45 e-2
$SVOL$	9.88 e-2	7.52 e-2

Table 7. Disturbance model parameter tolerance range (nearest tolerance limit is shown under min(TOL)).

Model	Parameter	Value	Min	Max	min(TOL)[%]
$\frac{LOAD(s)}{\alpha_r(s)}$	K	3.5	0	5.5	+57 %
	τ	0.727	0.0	∞	-100 %
	θ	0.278	0	1.389	-100 %
$\frac{LOAD(s)}{\alpha_f(s)}$	K	-20	-50	0	+100 %
	τ	0.734	0.1	1.5	-86 %
	θ	0	0	0.044	-
$\frac{LOAD(s)}{\phi_r(s)}$	K	0.25	0	1.5	-100 %
	τ	0.696	0.4	∞	-43 %
	θ	0.278	0	∞	-100 %
$\frac{LOAD(s)}{\phi_f(s)}$	K	0.28	0.21	0.55	-25 %
	τ	0.725	0.4	0.9	+24 %
	θ	0.056	0	0.083	+48 %
	x	5	0	11	-100 %
	y	10	8	17	-20 %

and the results are given in Table 6. FBFF control reduced the input standard deviation and the output root mean squared error compared to FB control. This shows that FBFF control requires less input effort and that it is able to track the setpoint better.

To investigate the allowable tolerance in the disturbance model parameters from (9), each parameter was adjusted and the FF controller recalculated using (10), until it causes FBFF control to be equal to or worse than FB control. The performance was considered worse when it results in larger peaks, oscillation, or a longer settling time. The results are shown in Table 7.

The allowable model deviation shown in Table 7 indicates that tolerances in the $LOAD/\phi_f$ model and the ratio y, destabilises the control the most. The ϕ_f FF control loop is the most important and needs to be well tuned. Deriving ϕ_r and ϕ_f from the measured α_r for control purposes works reasonably well. The same method can be followed to derive α_f, but since the ϕ_f controller plays the major role, it might be more practical to neglect the α_f controller completely (see Table 7).

6. CONCLUSION

This paper proposed a method to measure and reject disturbances caused by changes in the feed ore distribution to a grinding mill circuit. If the measurement of the fraction of rocks in the feed (α_r) is available, a FBFF controller ($G_{C-FF}(s)$) provides noticeable improvement over FB control, especially in terms of reducing deviation from the setpoint and the amount of input effort required (see Table 6). FBFF control could maintain system stability under conditions where FB control would become unstable.

Tuning the FBFF controller in real-world applications will be very difficult. The parameters, α_f, α_r, ϕ_f and ϕ_r can not be easily measured or manipulated individually to design and tune individual FF controllers. This severely limits the practicality of feed size disturbance FF controllers for industrial applications.

The presented size distribution measurement system can successfully segment and identify the size of touching ore in a static image taken under controlled conditions. A main drawback of the method is that the background between the ore must be visible, i.e. the method can only analyse a single-layer of ore. Further research is required to classify multi-layered ore on a moving conveyor belt. Possibilities include a machine learning approach and using a high shutter speed camera.

REFERENCES

Coetzee, L.C. (2009). *Robust Nonlinear Model Predictive Control of closed run-of-mine ore milling circuit.* Ph.D. thesis, Unversity of Pretoria.

Coetzee, L.C., Craig, I.K., and Kerrigan, E.C. (2010). Robust nonlinear model predictive control of a run-of-mine ore milling circuit. *IEEE Trans. Control Syst. Technol.*, 18(1), 222–229.

Dougherty, E.R. and Lotufo, R.A. (2003). *Hands-on morphological image processing*, volume 59. SPIE press, 3rd edition.

Fang, H.Y., Yang, J.H., and Chen, Q. (2018). Particle size distribution and energy consumption during impact crushing of single granite particles. *J. S. Afr, Inst. Min. Metall.*, 118, 555–561.

Hinde, A. and Kalala, J. (2009). The application of a simplified approach to modelling tumbling mills, stirred media mills and hpgr's. *Minerals Eng.*, 22(7-8), 633–641.

le Roux, J.D., Craig, I.K., Hulbert, D.G., and Hinde, A.L. (2013). Analysis and validation of a run-of-mine ore grinding mill circuit model for process control. *Minerals Eng.*, 43-44, 121–134.

Morrell, S. (2004). A new autogenous and semi-autogenous mill model for scale-up, design and optimisation. *Minerals Eng.*, 17(3), 437–445.

Morrell, S., Finch, W., Kojovic, T., and Jr, H.D. (1996). Modelling and simulation of large diameter autogeneous and semi-autogeneous mills. *Int. J. Mineral Process*, 44, 289–300.

Morrell, S. and Valery, W. (2001). Influence of feed size on ag/sag mill performance. *SAG2001, Vancouver, BC, Canada*, 203–214.

Napier-Munn, T.J., Morrell, S., Morrison, R.D., and Kojovic, T. (1999). *Mineral Communition Circuits: Their Operation and Optimisation.* JKMRC Monograph Series in Mining and Mineral Processing, 2nd edition.

Seborg, D.E., Edgar, T.F., Mellichamp, D.A., and Doyle, F. (2011). *Process Dynamics and Control.* John Wiley & Sons, Inc., 3rd edition.

Wei, D. and Craig, I.K. (2009). Grinding mill circuits - a survey of control and economic concerns. *Int. J. Mineral Process*, 90(1-4), 56–66.